Supplementary Information for “Tunable ultrastrong magnon–magnon coupling and spin Hall magnetoresistance in a 2D van der Waals antiferromagnet”

C. W. F. Freeman[1,2,*], Z. Xue[1], H. Youel[1], A.K. Budniak[3,4], H. De Libero[5], T. Thomson[5], M. Bosman[4,6], G. Eda[3,7,8], H. Kurebayashi[1,9,10] & M. Cubukcu[1,2,†]

April 12, 2024

Material Characterisation

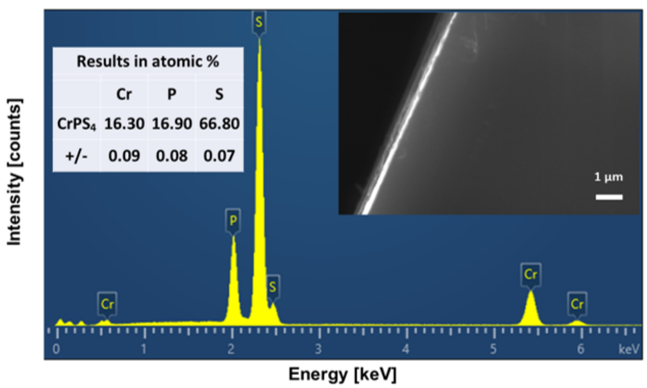

Figure S1: **Structural characterisation.** The EDS spectrum of bulk $CrPS_4$ registered with scanning electron microscope (SEM). All three elements: chromium, phosphorus, and sulfur are present in the sample. The inset shows an InLens micrograph of the crystals, where the series of spectra was recorded. The table presents the atomic composition, based on a few measurements. The Cr:P:S ratio is close to 1:1:4 further confirming receiving $CrPS_4$.

Spin dynamics measurements

Lorentzian Fit

Lineshape fitting shown in Fig. 2(d) in the main manuscript is carried out with derivated Lorentzian using the NanOsc fitting software, which uses the following Eq.:

$$\mathrm{FMR} = A\frac{4\Delta H\left(H-H_{res}\right)}{\left[4\left(H-H_{res}\right)^2+(\Delta H)^2\right]^2} - B\frac{(\Delta H)^2-4\left(H-H_{res}\right)^2}{\left[4\left(H-H_{res}\right)^2+(\Delta H)^2\right]^2} + \text{ slope} + \text{offset} \qquad \text{(S1)}$$

where FMR is the measured transmitted power derivate, ΔH is the linewidth and H_{res} is the resonant field, A and B and fitting constants.

[1] London Centre for Nanotechnology, University College London, London, WC1H 0AH, UK [2] National Physical Laboratory, Teddington, TW11 0LW, UK [3] Department of Physics, National University of Singapore, 117551, Singapore [4] Department of Materials Science Engineering, National University of Singapore, 117581, Singapore [5] Department of Computer Science, University of Manchester, Manchester, M13 9PL, UK [6] Institute for Materials Research and Engineering, Agency for Science, Technology and Research (ASTAR), 138634, Singapore [7] Department of Chemistry, National University of Singapore, 117543, Singapore [8] Centre for Advanced 2D Materials, National University of Singapore, 117542, Singapore [9] Department of Electronic and Electrical Engineering, University College London, London, WC1E 7JE, UK [10] WPI-AIMR, Tohoku University, 2-1-1, Katahira, Sendai 980-8577, Japan * uceecwf@ucl.ac.uk † m.cubukcu@ucl.ac.uk

H_E and γ as a function of temperature

In Fig. S2(a), we show that H_E decreases nonlinearly with temperature. Such a trend is expected for the temperature dependence with the value dropping to zero at the T_N.

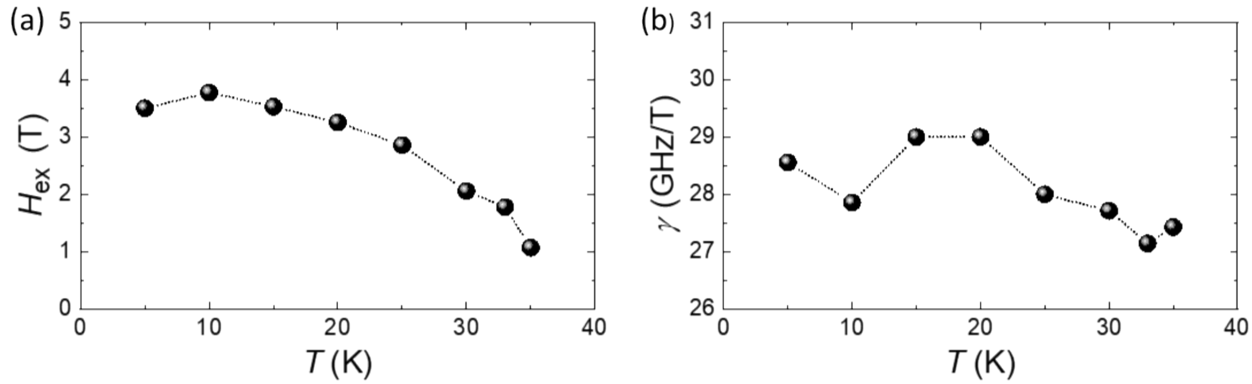

Figure S2: **Magnetic properties.** H_E (a) and γ (b) as a function of T.

In Fig. S2(b), we observe that γ is decreasing as a function of temperature from a maximum value of 29 GHz/T at 15K down to 27 GHz/T at 30 K.

Micromagnetic simulation

FMR micromagnetic simulations were performed using the Mumax^3 package [1]. $CrPS_4$ was modelled using a $5 \times 5 \times 25$ nm^3 cell grid with dimensions $150 \times 250 \times 50$ nm^3, which reflected approximate sample proportions of 3:5:1. The upper and lower cells in the out of plane direction were anti-ferromagnetically coupled with an exchange scaling of -38.4 and exchange stiffness of 10^{-12} J/m. Gilbert damping was set to 0.001 and the simulation temperature was held at 0 K.

The simulation is carried out using the magnetic parameters determined from magnetometry at 5 K. FMR spectra are obtained using sinc field pulses at an applied external field. The sinc pulse period was set to 10 ns and the time-varying magnetisation responses were Fourier transformed

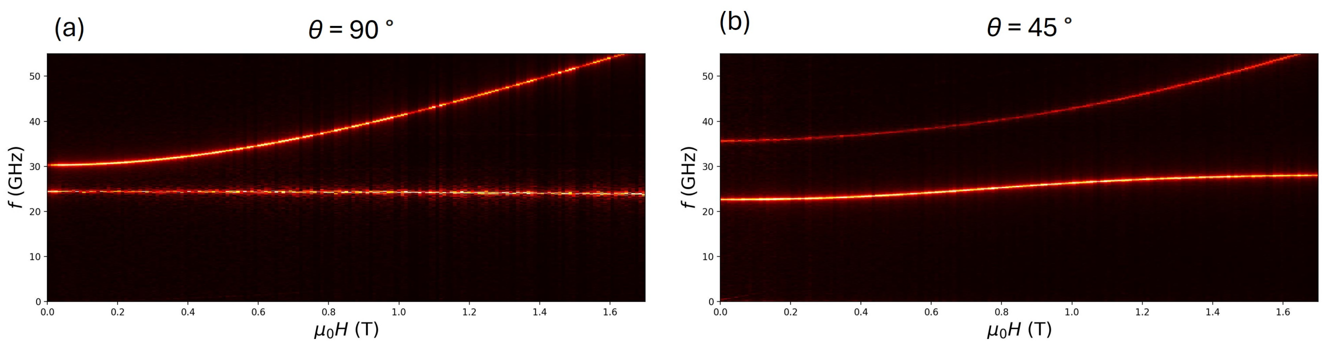

Figure S3: **Simulated Resonance Spectra**. MuMax^3 simulated resonance spectra with magnetic parameters at 5 K for the two angles with $\theta = 90$ ° zero coupling (a), and $\theta = 45$ ° maximimum coupling (b).

to obtain the final spectra. In Fig. S3(a), we observe no crossing of the modes and not magnon-magnon coupling as observed in Fig. 2(e) in the main manuscript. In Fig. S3(b), we show a good agreement to the experimental data at 5 K (Fig. S4(a)) and observe the symmetry breaking magnon-magnon coupling when the crystal is rotated 45°.

Temperature-dependent ultrastrong magnon–magnon coupling with an in-plane magnetic field at 45°

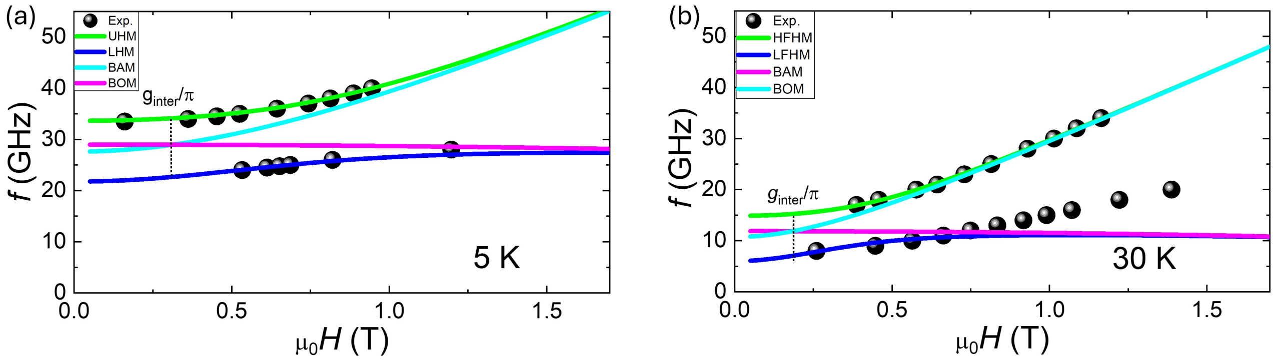

Figure S4: **Resonance spectras at different temperatures.** f dependent FMR results obtained at 5 K (a) and 30 K (b).

In Fig. S4, we show field dependent FMR spectra for two example temperatures 5 K (a) and 30 K (b). At temperatures above 25 K, the spectra obtained differ from the theoretical model used in this paper for high fields. In Fig. S4(b), we see a linearly increasing lower hybridised mode beyond the intersecting frequency of the two modes. Such a trend cannot be accounted for in the theoretical model. Through the field sweep technique used in this study it cannot be distinguished whether this is the LFHM mode not abiding by the theoretical model or whether this is a new mode e.g. spin wave mode. Further study with high field VNA or frequency sweeps could be used to understand this modes field dependence further at temperatures closer to the Neél temperature and would provide crucial understanding of the evolution or anisotropy and spin dynamics in this vdW antiferromagnet. This anomalous behaviour does not impact the findings of our study as the diversion from the theoretical trend occurs at fields significantly above the intersection where $g_{inter}/2\pi$ is taken, and hence will not impact the values obtained.

Electrical transport measurements

We present in Fig. S5 the R_{xy} results with fitting $R_{\text{xy}} = \Delta R_{\text{xy}} cos(\alpha)\sin(\alpha)$. The presence of a SMR like signal in R_{xy} confirms the Hanle magnetoresistance is not the origin of the SMR signal observed in Figure 4 (e-g) in the main text.

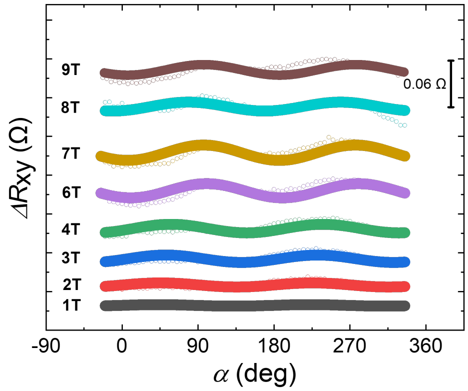

Figure S5: **The measured Rxy signal (open dots) and their fitting (lines) for a range of fields at 3 K**. The R_{xy} signal has a linear component that has been removed.

Comparison of Pt and Pt/$CrPS_4$/h-BN devices

Weak anti-localisation (WAL) occurs at low temperatures due to quantum interference from scattering at defects, leading to corrections to the resistance [2]. In the out-of-plane rotations, we observe a strong angular dependent signal at low temperatures as has been described previously by Oyonagi et al [3].

In Fig. S6(c) we see when rotating through angles β or γ we see the same angular dependence. This makes it difficult to determine the SMR amplitude using the β rotation at low temperatures and hence we focus on the in-plane rotation in the main text, which should have no WAL signal as described in [3].

In Fig. S6(d), we compare the ΔR_{xx} angular dependence for in-plane rotation of H, at 3 K and 9 T. We do not observe any comparable angular dependence in the bare Pt device in this orientation and hence the signal observed in the Pt/$CrPS_4$/h-BN device can be attributed solely to SMR.

Theory

To calculate the resonance frequencies as a function of field we follow the method set out by Li et al. [4] which we include for completeness here.

The free energy equation for orthorhombic anisotropy is proposed by Keffer et al. [5] where we set K_3 and K_4 to zero. The coordinate system adopted is displayed in Fig. S7 for H in plane with an angle θ from the y axis, where x, y, z corresponding to the a, b and c axis respectively. A rotation of coordinates into $\delta m_{r'}$, $\delta m_{\alpha'}$ and $\delta m_{\alpha'}$ is defined with respect to $\hat{m}_A$

Next the equilibrium equation is defined such that $\hat{m}_1$ aligns with the total effective field. The equilibrium equations are given by the following,

$$\begin{aligned} H\cos(\varphi-\theta) &= \left(2H_E - Ms + H_{A1}\sin^2\varphi + H_{A2}\cos^2\varphi\right)\sin\alpha \\ H\sin(\varphi-\theta) &= (H_{A2}-H_{A1})\sin\alpha\sin\varphi\cos\varphi \end{aligned} \tag{S2}$$

This is equation is solved numerically to find α and φ for values of H, the values are of the same value for $\hat{m}_B$.

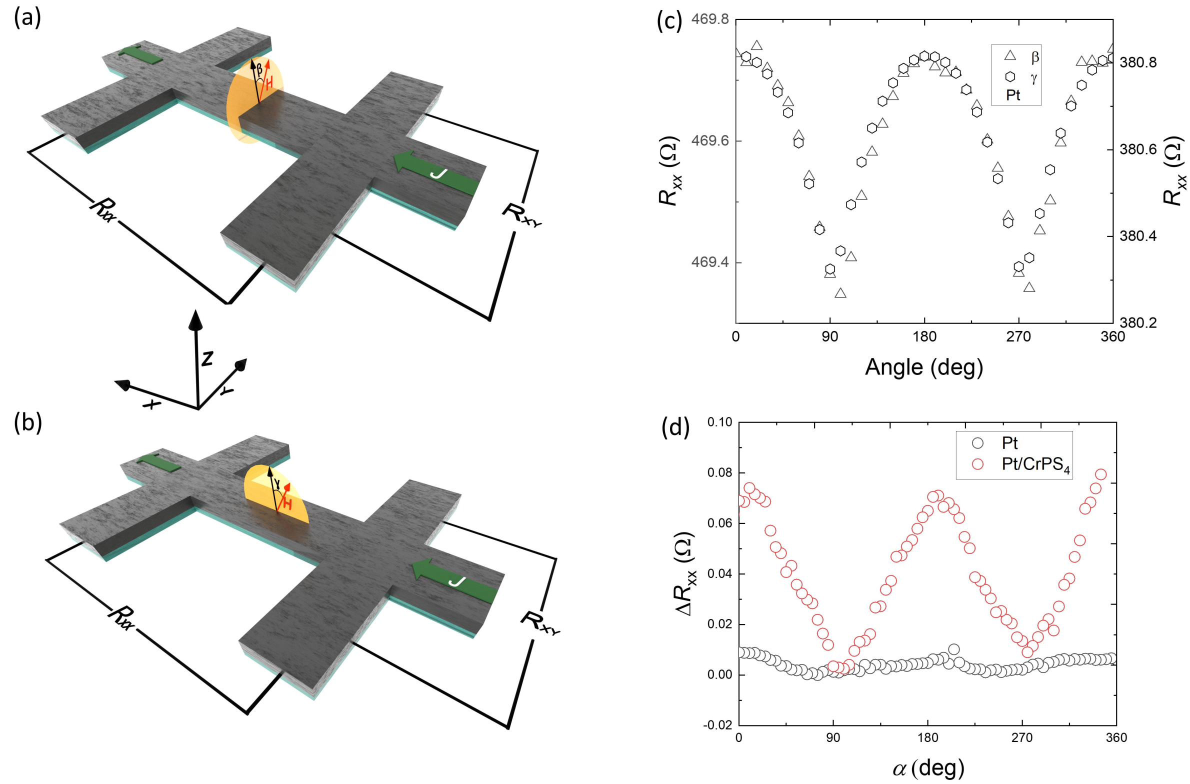

Figure S6: **Comparison between reference Pt and Pt/CrPS$_4$/h-BN device**. Diagram of two out-of-plane rotations with angles γ (a) and β (b). (c) Comparison of γ and β rotations for Pt device at 5 K and 9 T showing WAL. (d) Comparison of α rotation (in-plane) between the Pt/CrPS$_4$/h-BN device and Pt reference sample at 3 K and 9 T.

Next the LL equation (no damping term) is given for the two sublattices as defined in the main text Eq. 2.

This is then expanded with $\hat{m}_i = \hat{m}_i^e q + \delta m_i e^{i\omega t}$ $(i = A, B)$. where the latter term is the precession of the magnetic moments about the equilibrium position, resulting in

$$\begin{aligned} i\omega\delta m_i =& \mu_0\gamma\hat{m}_i^e q \times (H_E - M_s\delta m_i + H_E\delta m_j + M_s(\delta m_i\cdot\hat{z})\hat{z} + \\ & H_{A1}(\delta m_i\cdot\hat{x})\hat{x} + H_{A2}(\delta m_i\cdot\hat{y})\hat{y} i, j = A, B \end{aligned} \tag{S3}$$

Two new vectors are defined, namely

$$\begin{aligned} \delta m_+ &= \delta m_1 + C_{2y'}\delta m_2, \\ \delta m_- &= \delta m_1 - C_{2y'}\delta m_2, \end{aligned} \tag{S4}$$

where $C_{2y'}$ corresponds to a 180 degree rotation about the y' axis. Substituting into Eq. S3,

$$\begin{aligned} i\omega\delta m_\pm =& \mu_0\gamma\widehat{m}_1^{eq} \times \left(H^{eq}\delta m_\pm \pm H_E C_{2y}\delta m_\pm + M_S\left(\delta m_\pm\cdot\hat{z}\right)\hat{z}\right. \\ & + \frac{H_{A1}}{2}\delta m_\pm\left(\cdot\hat{x}\hat{x} + \left(\cdot C_{2y},\hat{x}\right)\left(C_{2y},\hat{x}\right)\right) + \frac{H_{A1}}{2}\delta m_\mp\left(\cdot\hat{x}\hat{x} - \left(\cdot C_{2y},\hat{x}\right)\left(C_{2y},\hat{x}\right)\right) \\ & + \frac{H_{A2}}{2}\delta m_\pm\left(\cdot\hat{y}\hat{y} + \left(\cdot C_{2y},\hat{y}\right)\left(C_{2y},\hat{y}\right)\right) + \frac{H_{A2}}{2}\delta m_\mp\left(\cdot\hat{y}\hat{y} - \left(\cdot C_{2y},\hat{y}\right)\left(C_{2y},\hat{y}\right)\right) \end{aligned} \tag{S5}$$

This can be represented as a matrix equation by the following,

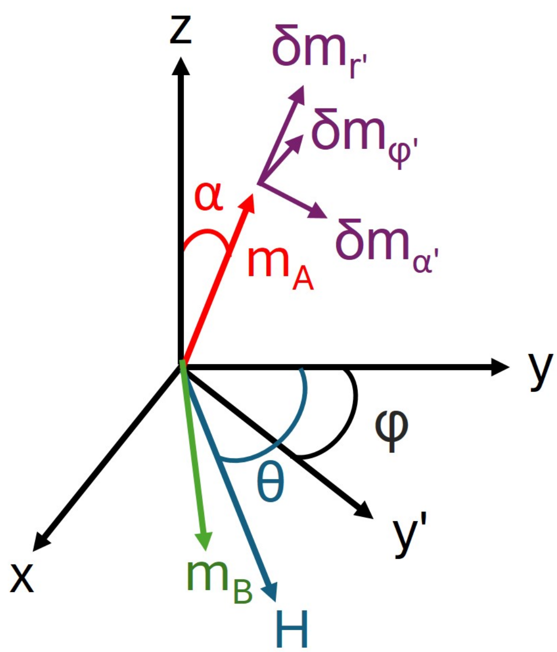

Figure S7: **Coordinate system for in-plane field equilibrium equation.**

$$iw\begin{pmatrix}\delta m_{+,\alpha\prime}\\ \delta m_{+,\varphi\prime}\\ \delta m_{-,\alpha\prime}\\ \delta m_{-,\varphi\prime}\end{pmatrix}=\mu_0\gamma\begin{pmatrix}0 & H_{o12} & H_{o13} & 0\\ H_{o21} & 0 & 0 & H_{o24}\\ H_{o31} & 0 & 0 & H_{o34}\\ 0 & H_{o42} & H_{o43} & 0\end{pmatrix}\begin{pmatrix}\delta m_{+,\alpha\prime}\\ \delta m_{+,\varphi\prime}\\ \delta m_{-,\alpha\prime}\\ \delta m_{-,\varphi}\end{pmatrix} \tag{S6}$$

where,

$$\begin{aligned}
H_{o12} &= M_s - H_{A1}\cos^2\varphi - H_{A2}\sin^2\varphi,\\
H_{o13} &= (H_{A1} - H_{A2})\cos\alpha\sin\varphi\cos\varphi,\\
H_{o21} &= (2H_E - M_S)\cos^2\alpha + H_{A1}\cos^2\alpha\sin^2\varphi + H_{A2}\cos^2\alpha\cos^2\varphi,\\
H_{o24} &= (-H_{A1} + H_{A2})\cos\alpha\sin\varphi\cos\varphi,\\
H_{o31} &= (H_{A1} - H_{A2})\cos\alpha\sin\varphi\cos\varphi,\\
H_{o34} &= -\left((2H_E - M_S) + H_{A1}\cos^2\varphi + H_{A2}\sin^2\varphi\right),\\
H_{o42} &= (-H_{A1} + H_{A2})\cos\alpha\sin\varphi\cos\varphi,\\
H_{o43} &= 2H_E\sin^2\alpha - M_S\cos^2\alpha + H_{A1}\cos^2\alpha\sin^2\varphi + H_{A2}\cos^2\alpha\cos^2\varphi.
\end{aligned} \tag{S7}$$

Solutions to this are given through simple computation of the real part of the eigenvalues of $\boldsymbol{A} = i\mu_0\gamma\boldsymbol{H}_o$ the resonance frequency of the two modes for H can then be computed and is used to fit to the experimental resonance spectra. The derivation for the matrix equation for an out of plane field follows the same derivation with the addition of a monoclinic anisotropy term and is detailed fully in [4].

References

[1] Vansteenkiste, A. *et al.* The design and verification of mumax3. *AIP advances* **4** (2014).

[2] Jana, S., Senapati, T., Senapati, K. & Samal, D. Multiband character revealed from weak antilocalization in platinum thin films. *Phys. Rev. B* **107**, 035127 (2023).

[3] Oyanagi, K. *et al.* Paramagnetic spin hall magnetoresistance. *Phys. Rev. B* **104**, 134428 (2021).

[4] Li, W. *et al.* Ultrastrong magnon–magnon coupling and chirality switching in antiferromagnet $CrPS_4$. *Adv. Func. Mat.* **33**, 2303781 (2023).

[5] Keffer, F. & Kittel, C. Theory of antiferromagnetic resonance. *Phys. Rev.* **85**, 329 (1952).